JOURNAL OF GEOPHYSICAL RESEARCH, VOL. 107, NO. D15, 10.1029/2001JD000324, 2002

SST-forced surface wind variability in the tropical Atlantic: An empirical model

Chul Chung,[1] Sumant Nigam, and James Carton
Department of Meteorology, University of Maryland, College Park, Maryland, USA

Received 4 January 2001; revised 11 October 2001; accepted 18 October 2001; published 6 August 2002.

[1] Simple dynamical models developed for the tropical Pacific surface winds may not be directly applicable in the Atlantic in view of the basin's different geometry and size and the potential impact of deep heating from over the adjacent African and South American continents. As simple dynamical models generate surface winds from sea-surface temperature (SST), it is worth ascertaining the extent to which monthly surface winds over the tropical (30°S–30°N) Atlantic are driven by this sector's own SST variations. A procedure is developed to separate this internally driven (i.e., by tropical Atlantic basin SSTs) component of the surface wind field from those induced by changes external to this tropical basin. Our analysis shows the internally driven component to dominate wind variability only within the equatorial (10°S–10°N) Atlantic. In contrast, Pacific surface winds driven by the tropical Pacific basin SSTs dominate variability across the tropical Pacific. The vertical structure of atmospheric diabatic heating linked with the leading modes of internally driven variability in the two basins (e.g., Pacific El Niño and the Atlantic Niño) is compared to assess the suitability of hypotheses underlying simple dynamical models. The potential limitations of these models, particularly, in the tropical Atlantic, motivated the development of an empirical model for Atlantic surface-wind variability. The model is based on rotated principal component analysis (RPCA) of the internally driven component of interannual variability in the tropical Atlantic basin. The empirical model is constructed from RPCA analysis of combined SST and surface wind anomalies of individual calendar months (from COADS data set) and outperforms the simple dynamical models. The model's performance is also compared to an empirical model based on the singular value decomposition analysis of SST and surface winds. *INDEX TERMS:* 3339 Meteorology and Atmospheric Dynamics: Ocean/atmosphere interactions (0312, 4504); 4215 Oceanography: General: Climate and interannual variability (3309); 3374 Meteorology and Atmospheric Dynamics: Tropical meteorology

1. Introduction

[2] The trade-wind systems of the tropical Atlantic and eastern Pacific are similar in several respects. Both migrate seasonally in conjunction with the seasonally varying SST. Both basins show a single zone of trade-wind convergence which is generally located northward of the equator. The divergent Hadley circulations associated with these Inter-Tropical Convergence Zones (ITCZ) generate subsidence both to the north and south, and contribute to the development of stratus clouds and the subtropical anticyclones in sea level pressure; the latter are forced also to an extent by the Rossby wave descent induced by deep monsoonal heating over continents to the east [*Hoskins*, 1996]. Both basins also exhibit rather robust and similarly structured annual-cycle variability in SST and surface winds in the eastern equatorial sector [e.g., *Nigam and Chao*, 1996].

[3] However, there are also differences between the two basins. Interannual SST variability in the tropical Atlantic is rather modest in comparison with that in the tropical Pacific [e.g., *Philander*, 1990]. Smaller SST amplitudes in the Atlantic (~1/3 of the Pacific ones) can allow its surface-wind field to be influenced to a greater extent by disturbances originating in other tropical sectors (e.g., El Niño conditions in the central/eastern Pacific) and in the extratropics (e.g., from the North Atlantic Oscillation). Such externally forced surface winds are expected to induce weak SST variability in the equatorial Atlantic, at least on the short timescale. Externally generated winds can however be instigators of robust variability on longer time-scales, e.g., Atlantic Niño, which is sustained by air-sea interaction within the tropical Atlantic basin [*Zebiak*, 1993; *Carton et al.*, 1996]. Differences in interannual SST variability amplitudes between the two basins can also lead to different vertical structures of diabatic heating and to different depths of the trade-wind boundary layers—both having implication for simple dynamical models.

[1] Currently at Center for Clouds, Chemistry, and Climate, Scripps Institution of Oceanography, La Jolla, California, USA.

0148-0227/02/2001JD000324$09.00

[4] From the viewpoint of simple dynamical models for tropical Atlantic surface winds, one is more interested in the wind variability forced by this basin's own SST anomalies, i.e., in the internally driven component. Empirical models, on the other hand, can be devised to capture both the internal and externally driven components of wind variability. The existence of wind variability that is in balance with local changes in SST in the tropical Atlantic has been a topic of active discussion for over twenty years ([*Merle*, 1980; *Moura and Shukla*, 1981] being two of the interesting early studies). Observational studies beginning with *Merle* [1980] have shown that the eastern tropical Atlantic is unusually warm in boreal summers every few years. The eastern thermocline is depressed by about 20 meters from its climatological seasonal depth, the trade winds weaken in the central basin, and the ITCZ, which is normally located well north of the equator in this season, is shifted southeastward toward the eastern equator and strengthens during these summers [*Philander*, 1986; *Servain*, 1991; *Ruiz-Barradas et al.*, 2000]. This mode of variability, which modeling studies strongly suggest involves local air-sea interaction [e.g., *Zebiak*, 1993; *Carton and Huang*, 1994; *Dommenget and Latif*, 2000], is referred to as the Atlantic Nino in this analysis.

[5] On somewhat longer time-scales, the ITCZ undergoes meridional displacements in response to non-seasonal variations in the interhemispheric gradient of SST [*Hastenrath*, 1991; *Ruiz-Barradas et al.*, 2000; *Chiang et al.*, 2001], resulting in dipole-like variability in diabatic heating and precipitation [*Ruiz-Barradas et al.*, 2000; *Xie and Saito*, 2001]. The associated change in positions of the northeast and southeast trades generates surface heat-flux anomalies, which, in turn, feedback on the interhemispheric SST gradient [*Carton et al.*, 1996; *Chang et al.*, 1997, 2001]. Together, these features describe a mode of variability that is referred to here as the interhemispheric mode. It is however important to note that variability similar to both modes can be produced by processes external to the Atlantic sector as well [*Lanzante*, 1996; *Enfield and Mayer*, 1997; *Mehta*, 1998; *Tanimoto and Xie*, 1999].

[6] Distinguishing between the internal and externally generated components of tropical Atlantic variability is one of the key tasks of this study. A method to extract the internally driven component is discussed, and applied to the *DaSilva et al.*'s [1994] COADS record. The extraction facilitates the construction of an empirical model of locally driven surface wind variability, and allows a more reasonable evaluation of simple dynamical models.

[7] We examine the applicability of two simple dynamical models of the tropical atmosphere, the *Gill* [1980] and the *Lindzen and Nigam* [1987] models, to the Atlantic sector. The central premise of the Gill model is that deep convective heating drives surface winds in the tropics. Shortcomings in Gill-model's dynamics in the Pacific sector were illustrated in *Nigam and Shen* [1993], where horizontal structure of the deep convective heating anomalies was specified using the ENSO related Outgoing Longwave Radiation (OLR) anomalies. The modeled Pacific surface winds were found to be deficient in several respects, but particularly noteworthy was the discrepancy in the zonal and meridional wind contributions to the surface divergence anomaly: in nature, the $\partial v/\partial y$ term is dominant, while in the Gill model's solution to quasi-perfect forcing (ENSO covariant OLR anomalies), the $\partial u/\partial x$ term was dominant (see Figures 2, 3, and 12 of that paper). Differences in SST variability as well as differences in subsidence zones between the two basins lead to different vertical structures of diabatic heating, which can further limit the applicability of this model in the Atlantic.

[8] The Lindzen-Nigam model, in contrast, is based on the premise that horizontal temperature distribution beneath the trade inversion reflects the underlying SST distribution because of vertical mixing by trade-cumuli. In this model, the hydrostatically generated sea level pressure gradients drive the tropical near-surface winds. The model is not without its shortcomings, the principal one of which is the lack of dependence of the mean inversion height on SST. *Battisti et al.* [1999] have also argued, correctly, that in view of the capping inversion, a reduced gravity formalism ought to be employed. They show that this leads to the same solutions but with a more reasonable (longer) thermal damping time-scale [$(\varepsilon_T)^{\bullet 1}$ in the original model]. But most importantly, the model requires the existence of a well-mixed boundary layer (capped by an inversion), which is generally present only in the central/eastern sectors of the tropical oceans, under the subsiding branches of the divergent Walker and Hadley circulations. Coarse vertical sampling of the planetary boundary layer (PBL) in the reanalysis data sets ($\Delta p = 75$mb, at best) however precludes a comparison of PBL depths in the two basins.

[9] In view of the limitations of simple dynamical models, including their potential suitability in only some sectors of the tropical basins, we develop an empirical model for the internally driven component of Atlantic surface-wind variability. The model is based on rotated principal component analysis of the internally generated interannual variability in individual calendar months of the COADS record. The model's performance is compared to the original Gill and Lindzen-Nigam models in the Atlantic basin, and briefly to an alternate empirical model based on singular value decomposition analysis (following *Chang et al.* [1997]). Both empirical models are found to outperform the dynamical models.

[10] The paper is organized into six sections. Section 2 briefly describes the various data sets. The internally driven surface-wind variability is extracted in section 3. The vertical structure of diabatic heating associated with ENSO variability in the Pacific and Niño variability in the Atlantic are compared in section 4. The empirical model is developed in section 5, and its performance is compared with that of simple dynamical models in section 6. Summary and concluding remarks follow in section 7.

2. Data Sets

2.1. Revised COADS

[11] The revised Comprehensive Ocean-Atmosphere Data Set (COADS) used in this study was developed by *Da Silva et al.* [1994], from the objective analysis of individual COADS observations on a 1° grid during January 1945–December 1993. The data set reduces the wind speed bias and artificial wind speed trends associated with an erroneous Beaufort equivalent scale. However, like other objectively analyzed COADS data sets, it suffers from

sparseness of observations in the central/eastern equatorial Pacific where "less than five wind observations per month per 1° × 1° box" is not uncommon, particularly in the early part of the data record.

[12] Monthly SST and surface wind anomalies are defined relative to the 1950–93 monthly climatology. The anomalies are smoothed with a 9-point smoother and linearly interpolated onto a 2.5° grid. The wind anomalies exhibited a long-term trend at some grid points [cf. *Clarke and Lebedev*, 1996]; as this was believed to be spurious, the winds and SSTs were linearly detrended at each point in each calendar month.

2.2. ECMWF Reanalyses

[13] The 6-hourly initialized European Centre for Medium-Range Weather Forecasts (ECMWF) reanalysis archived at NCAR on a 2.5° global grid and at 17 pressure levels for the January 1979 to December 1993 period were used to compute the monthly-mean fields and the sub-monthly transients from which the 3D diabatic heating was residually diagnosed from the thermodynamic equation [see *Nigam et al.*, 2000, section 3]. Diabatic heating anomalies were obtained on a 5.0° × 2.5° longitude-latitude grid, relative to the 1979–93 monthly climatology.

2.3. NCEP Reanalyses

[14] The 6-hourly National Center for Environmental Prediction (NCEP) reanalysis for the 1958–1993 period [*Kalnay et al.*, 1996] are available on a 2.5° global grid and at 17 pressure levels. The data set contains diabatic heating generated during a 6-hour model forecast starting from each time step's reanalysis circulation. However, in view of potential differences between the model produced and the reanalysis-consistent heating, and in order to directly compare with the heating diagnosed from ECMWF reanalyses, diabatic heating was residually diagnosed from the NCEP reanalyses as well. Diabatic heating anomalies are obtained on the same 5.0° × 2.5° grid but relative to the 1979–93 monthly climatology in this case.

3. Extraction of Internally Driven Variability

[15] Surface wind variability generated by each basin's tropical SST anomalies is referred to as the internally driven component. The perturbation of tropical Atlantic winds by ENSO variability in the Pacific (the tropical bridge [*Klein et al.*, 1999]) and the impact of the North Atlantic Oscillation on the basin's tropics [*Xie and Tanimoto*, 1998]—impacts generated from remote forcing—are accordingly characterized as the externally forced component of tropical Atlantic wind variability. Note that over time periods longer than a month, the two components can contribute to each other's generation. For example, SST anomalies produced by externally forced winds can, in turn, generate local winds and, possibly, a coupled response. A separation strategy based on both contemporaneous structure and temporal evolution would be preferable, but its development is beyond the scope of this study.

[16] The difference between internally and externally forced components of variability is illustrated in Figure 1, which shows two modes from the RPCA analysis of combined variability of the tropical (30°S–30°N) Atlantic SST, and surface zonal and meridional winds (i.e., SST + u + v). Each of the three variables is scaled so as to have the same spatially integrated variance (see *Chung and Nigam* [1999a] for further analysis details); the principal components are rotated using the VARIMAX criterion [e.g., *Horel*, 1981]. The mode describing sub-decadal timescale ocean-atmosphere interannual variability in the tropical Atlantic basin ("Atlantic Niño" [see e.g., *Carton and Huang*, 1994; *Ruiz-Barradas et al.*, 2000]) is shown in Figure 1a. It is the 4th leading mode, and explains 4.4% of the combined variance. This mode would be classified as "internally driven" because the surface winds appear to be generated by the underlying SST gradients [cf. *Wagner and Da Silva*, 1994]. In contrast, the leading mode (Figure 1b), which explains 7.2% of the variance, has substantially weaker SST amplitudes, and a wind pattern that cannot be readily explained by this basin's SST distribution; the SST pattern, on the other hand, can be accounted for by the impact of wind speed on local evaporation and vertical mixing. In our scheme, this mode would be classified in the "externally driven" category.

[17] Comparison of Figures 1a and 1b suggests that the externally driven wind variability modes may be characterized by strong wind and weak SST amplitudes, while the internally driven ones are likely to exhibit weak wind and large SST amplitudes. The latter are also generally dominated by lower frequencies, whereas the externally driven ones can exhibit both lower (as in case of ENSO's contemporaneous impact on the Atlantic) and higher frequencies.

[18] Extraction of internally driven wind variability is quite challenging. If SST and surface wind observations were available at sub-monthly resolution (e.g., weekly) one could attempt extraction by examining the lead/lag relationship between SST and wind anomalies. The monthly data is however of little use in such analysis, as much of the wind response to SST is set up on weekly timescales. While a unique and robust extraction strategy still eludes us, our preliminary attempt to separate the internally and externally driven variability is based on the RPCA analysis of combined SST and surface wind variability.

[19] We classify each mode obtained from this analysis in one of the two categories, based on the very different ratios of the wind-to-SST amplitudes (see Figure 1). Taking advantage of this feature, we define an index (α) to objectively measure this ratio for each mode: $\alpha = \int(u^2 + v^2)dA / \int T^2 dA$.

[20] We rotated 70 loading vectors (EOFs), which together explained nearly 85% of the combined variance in the tropical Atlantic. For these 70 modes, α ranged from 0.3 to 240.6 $m^2\ s^2\ K^2$, and for the two modes shown in Figures 1a and 1b, α = 0.71 and 171.44, respectively. The externally driven wind variability modes are thus characterized by large α values. The 70 modes were sequenced using the α index, and the 15 leading ones (α ranging from 240.6 to 50.7) were tagged as externally driven. The cut-off at 15 was based on visual inspection of the modal wind/SST relationship, which indicated the 16th and higher modes ($\alpha \leq 29.1$) to be more in the internally driven category. While the cut-off at mode 15 is somewhat subjective, cut-offs at neighboring values have little impact

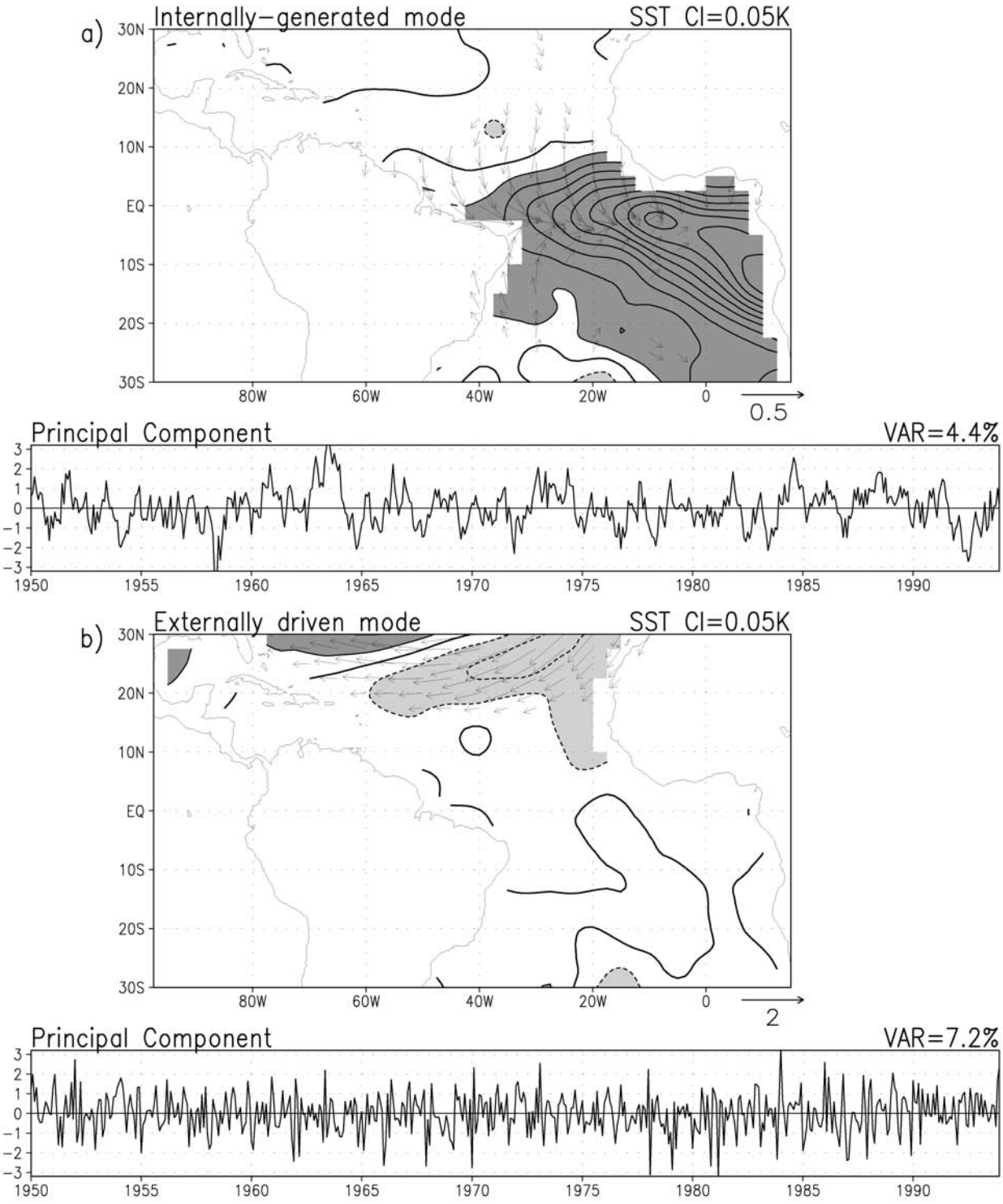

Figure 1. Rotated principal component analysis of the combined interannual variability of COADS SST + u + v during 1950–93 (a) an internally driven mode (Atlantic Niño) and its principal component and (b) an externally driven mode and its principal component. SST patterns are depicted using the contour interval and shading threshold of 0.05K, with zero contours thickened. Surface winds are superimposed on SST patterns using indicated vector scales (0.5 m/s in the top and 2.0 m/s in the bottom panel). The percentage of combined variance explained by each mode is shown above the principal component panel.

on subsequent analysis as these modes explain only a small percentage of the variance; for example, mode 16th explains 0.61%, and mode 17th 0.63% of the domain variance.

[21] The 15 externally driven modes, on the other hand, are quite efficient at explaining variance, as all 15 of them are found among the 22 leading modes (sequenced using explained variance). The variability not included in the 70 leading modes is therefore unlikely to be in the externally driven category. We thus subtract the surface-wind (and SST) variability associated with these 15 modes from the original anomaly records to define the internally driven component. The subtraction includes the SST component, because otherwise wind and SST would not be in balance. This is however of little consequence as the SST component in all 15 modes is very weak.

[22] The contribution of the internally driven component of surface zonal-wind variability in the tropical Atlantic is shown in Figure 2. Zonal wind is chosen for this illustration in view of its dominant role in driving oceanic variability in the tropics. The standard deviation of the internally driven component and the total zonal wind anomalies is computed, and their ratio is displayed in Figure 2c. That the equatorial (10°S–10°N) Atlantic winds are largely internally driven (ratio/90%) is evident and expected; surface winds in the southern tropical (10°S–25°S) Atlantic adjacent to the African coast are also mostly driven by tropical Atlantic SSTs. The off-equatorial regions, on the other hand, are dominated by the externally driven component which accounts for more than half of the standard deviation at 20°N and beyond. The counterpart figures for meridional wind and sea level pressure anomalies show features similar to those in Figure 2c.

[23] The extent of dominance of the internally driven wind component in the Pacific was also examined by repeating the above analysis in the tropical Pacific basin (Figure 3). Comparison of Figures 3 and 2c indicates that the Pacific basin (30°S–30°N) zonal winds are even more strongly internally driven, particularly, in the off-equatorial latitudes. The contrast between the basins suggests that the surface-wind modeling strategies for the two basins will likely be different in some respects.

[24] An actual example of the internally and externally driven components of wind variability in the tropical Atlantic is shown in Figure 4. The detrended surface-wind anomaly in August 1987 is displayed in the top panel. This month is chosen because of the sizable projection of both the Atlantic Niño (Figure 1a) and dipole [e.g., *Chang et al.*, 1997] modes during this period. This is also the month for which solutions of simple dynamical and empirical models are displayed later, although the empirical model's performance is evaluated more comprehensively, via verification statistics on model solutions for all available months. Comparison of Figures 4a and 4b shows that the internally driven component accounts for a substantial portion of the August 1987 surface wind anomalies—perhaps, more significantly in the off-equatorial region than anticipated on the basis of Figure 2c—due to sizable projections of the Niño and dipole modes in this month. The externally driven wind component is notable poleward of 20°N, particularly, in zonal wind anomalies.

4. Heating Vertical Structure

[25] The vertical distribution of diabatic heating associated with ENSO variability in the Pacific and Niño variability in the Atlantic is compared in this section in order to further characterize the structure of internally driven variability in the Atlantic. In addition to the basin intercomparison, the Atlantic heating structure in the two reanalyses is compared in the overlapping period (1979–93) of the data sets to ascertain the robustness of key features of the heating distribution.

4.1. Atlantic Sector

[26] *Ruiz-Barradas et al.* [2000] have documented the heating structure associated with the Atlantic Niño mode, using heating anomalies diagnosed from the 1958–93 NCEP reanalysis. Their Figure 4a shows that away from the adjoining continents, the equatorial heating-maximum in the Atlantic occurs in the lower troposphere (600–700mb)—and not in the middle and upper troposphere as in case of ENSO variability in the Pacific [*Nigam et al.*, 2000].

[27] The heating structure is examined here in a shorter record (1979–93) since both NCEP and ECMWF reanalyses are available in this 15-year period. The 3D diabatic heating is residually diagnosed from the thermodynamic equation, as noted before. The credibility of diagnosed heating has been ascertained in the ENSO context, both by comparison of the vertically averaged heating with the *Xie-Arkin* [1997] precipitation anomalies in the deep tropics (where condensation heating is dominant [*Nigam et al.*, 2000]), and by examination of the dynamical consistency of diagnosed heating and large-scale circulation (from diagnostic modeling in *Nigam and Chung* [2000]).

[28] The 1979–93 period heating anomalies linked to Niño variability in the Atlantic and ENSO variability in the Pacific are calculated from regression with the modes' principal components. The latter are obtained from separate RPCA analysis of Atlantic and Pacific basin variability in the longer 1950–93 period, as noted earlier. Linear regression against truncated principal components was deemed preferable to RPCA analysis of the truncated data set (which could alias variability structure, perhaps, more easily).

[29] The equatorial (4°S–4°N) heating associated with Atlantic Niño variability is shown in Figures 5a and 5b. The striking features in the top two panels are the magnitude of heating differences over the adjoining continents, and the variable level of the heating-maximum across the Atlantic basin. Heating reaches its maximum at a higher level (~400mb) in the western Atlantic, and the heating maximum slopes downward toward the east, as evident, particularly, in the NCEP heating structure (Figure 5a). Such a distribution of heating-maximum is not unexpected since it is likely controlled by the distribution of total (climatological + anomalous), and not just the anomalous SST. The variable level of the heating-maximum, and in particular, its location in the lower troposphere (p/700 mb) over the central Atlantic sector, suggests that simple dynamical models driven by mid-tropospheric heating may not be suitable in some Atlantic sectors.

[30] Unlike the oceanic sector where heating estimates are generally in accord, heating anomalies over the adjoining continents exhibit large discrepancies, with the ECMWF

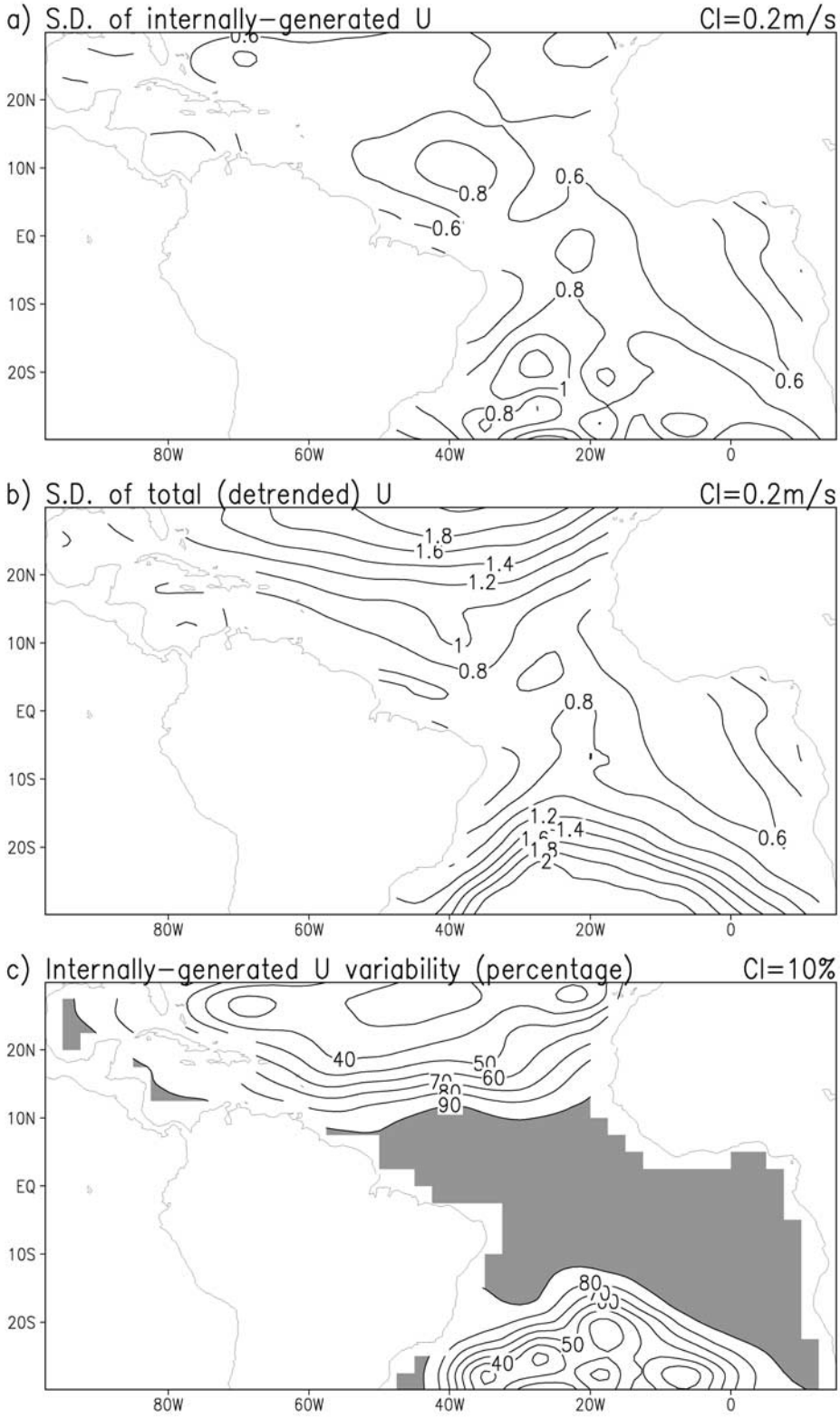

Figure 2. Standard deviation of monthly surface zonal winds during 1950–93 for (a) the wind component driven by tropical Atlantic SST (i.e., the internally driven component), (b) the total wind anomaly, and (c) the ratio of a-to-b, expressed as percentage. Figure 2c represents the magnitude of internally driven wind variability as percentage of total variability. Values greater than 90% are shaded.

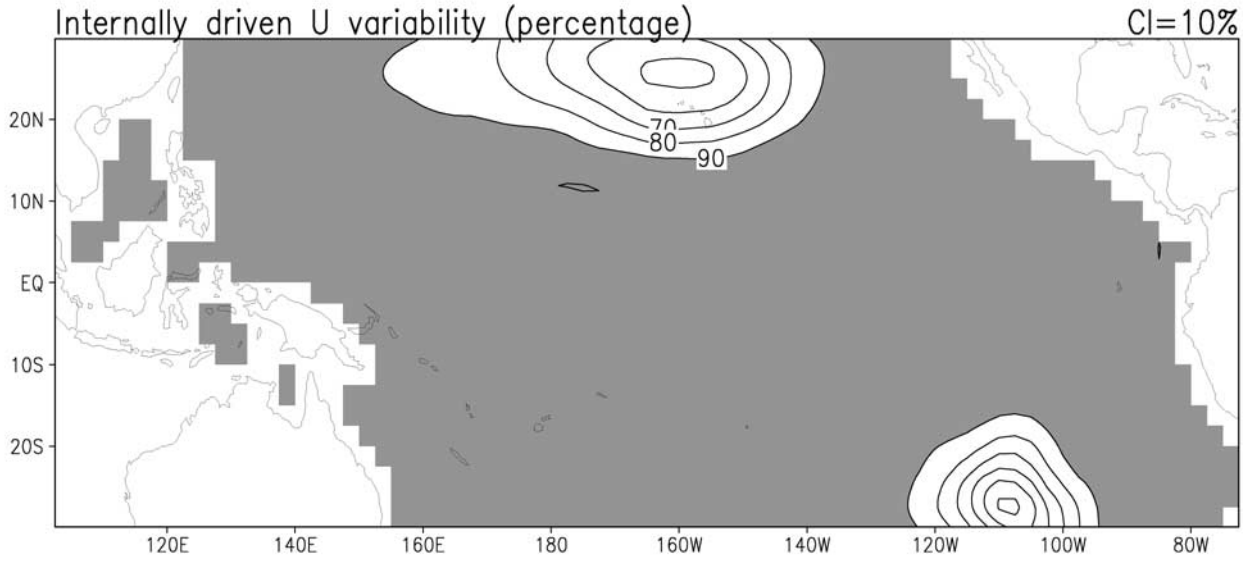

Figure 3. Magnitude of the internally driven Pacific wind variability expressed as percentage of total variability. Values greater than 90% are shaded, as in Figure 3.

one being much stronger. Since heating anomalies are calculated from the same period (1979–93) climatology in both cases, and the Atlantic Niño anomalies (Figures 5a–5b) generated by regression against the same principal component (Figure 1a), the discrepancies are not related to the analysis methodology. In the bottom panel of Figure 5, the vertically averaged (200–1000mb) heating anomalies are compared with the corresponding Xie-Arkin precipitation anomalies. Since the latter represent latent heating, this comparison may help understand the causes of the discrepancies over land, where heating is deep and of condensational origin. To the extent that Xie-Arkin precipitation estimates are realistic over land, Figure 5c suggests that the deep Amazonian heating implicit in ECMWF reanalysis may be unrealistic. On the other hand, the precipitation estimate corroborates the heating structures over the oceanic sector.

4.2. Pacific Sector

[31] For purposes of comparison, the distribution of diabatic heating associated with ENSO variability in the 1979–93 period is shown in Figure 6. The ENSO heating anomalies are about twice as strong as the Atlantic Niño ones, and the NCEP and ECMWF based estimates are more consistent, as well. Both heating anomalies moreover peak in the mid-troposphere (400–500mb) across much of the equatorial Pacific. While heating anomalies over the continents (Maritime included) continue to be stronger in the ECMWF estimate, the discrepancies between the two estimates are evidently more modest. Comparison of the heating vertical structures in the central equatorial Pacific shows the ECMWF estimate to be considerably stronger in the lower troposphere (p/700mb) as well, where it exhibits a local maximum (see *Nigam et al.* [2000] for more details).

[32] The Xie-Arkin precipitation anomalies linked to ENSO variability during 1979–93 are shown in Figure 6c along with profiles of the two vertically averaged heating estimates. There is greater consistency among various profiles in the Pacific sector, with the correspondence between heating estimates being particularly notable. Note that both estimates show ENSO heating to be strongest eastward of the dateline, but the Xie-Arkin precipitation anomalies are largest just to the west of it.

5. Empirical Model for Atlantic Surface Winds

[33] In view of the unique structure of the tropical Atlantic basin—South American and African landmasses protruding in the Southern and Northern tropics, respectively—the vertical structure of diabatic heating anomalies varies considerably across the Atlantic longitudes. The protruding landmasses moreover exert substantial influence on surface-wind variability over the tropical Atlantic ocean, with potential feedback. Thus, unlike the tropical Pacific where the dynamically simplified ocean-atmosphere models can simulate some features of low-frequency variability (e.g., ENSO), simulation of climate variability in the Atlantic sector is more challenging: The interaction of ocean and atmosphere with the adjoining landmasses must be additionally modeled. Besides, the simplified atmospheric models may be unsuitable in some sectors of the tropical Atlantic on account of significant variations in the heating vertical structure. Such concerns motivated the development of an empirical model of Atlantic surface-wind variability.

[34] The construction of an empirical (statistical) model of surface wind/windstress is not novel in itself, as such models have been used in the coupled modeling of Pacific interannual variability. *Barnett et al.* [1993] developed a model based on EOFs of individual fields while *Syu et al.* [1995] based their model on singular value decomposition of the covariance between Pacific SST and surface wind stress anomalies. Such a model has been developed for the tropical Atlantic as well [*Chang et al.*, 1997].

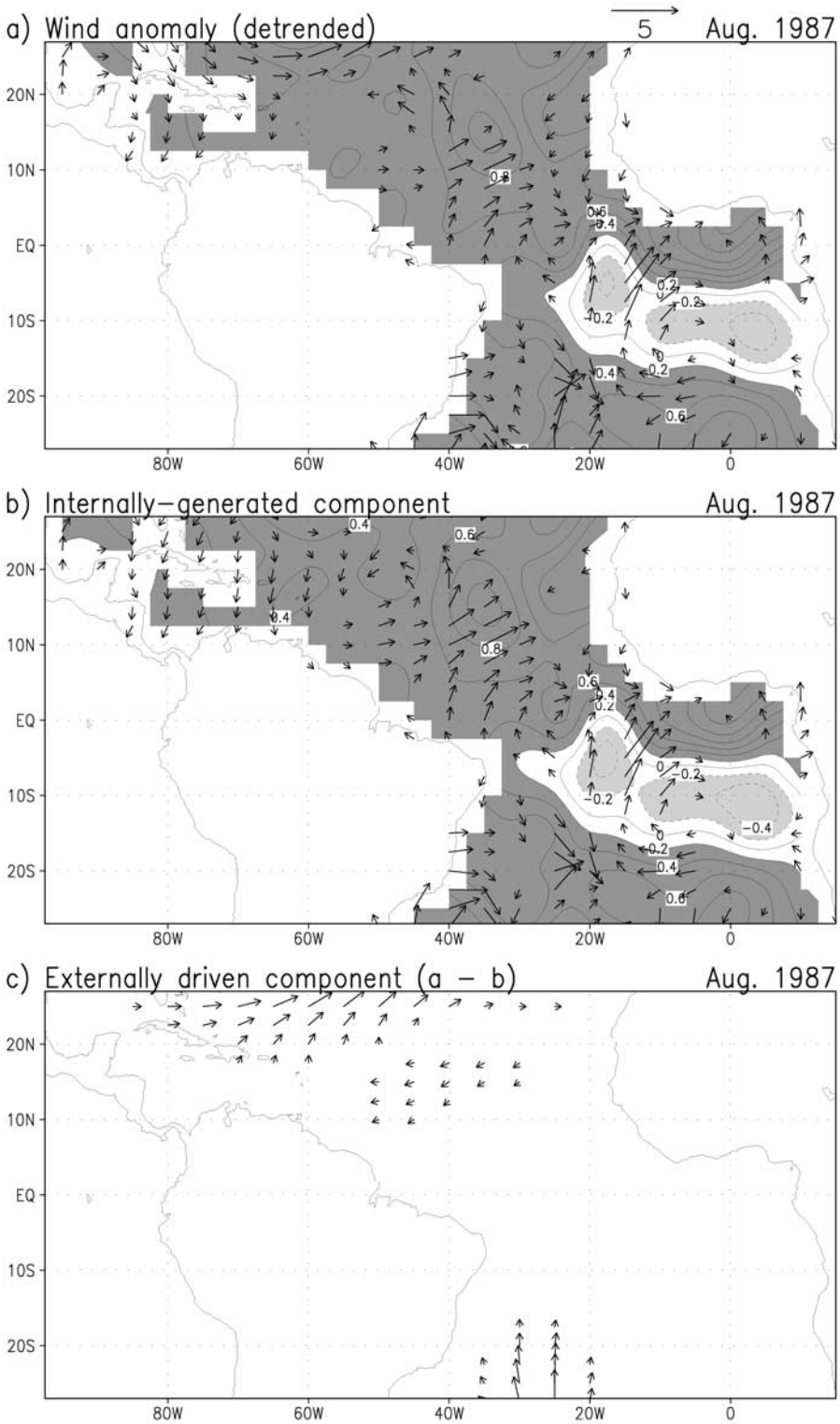

Figure 4. Surface wind anomaly for August, 1987 (a) from detrended COADS, (b) its internally driven component, and (c) the difference (ab). The vector scale is indicated in the top panel. The underlying SST anomalies are displayed in Figures 4a to 4c using a contour interval of 0.1 K.

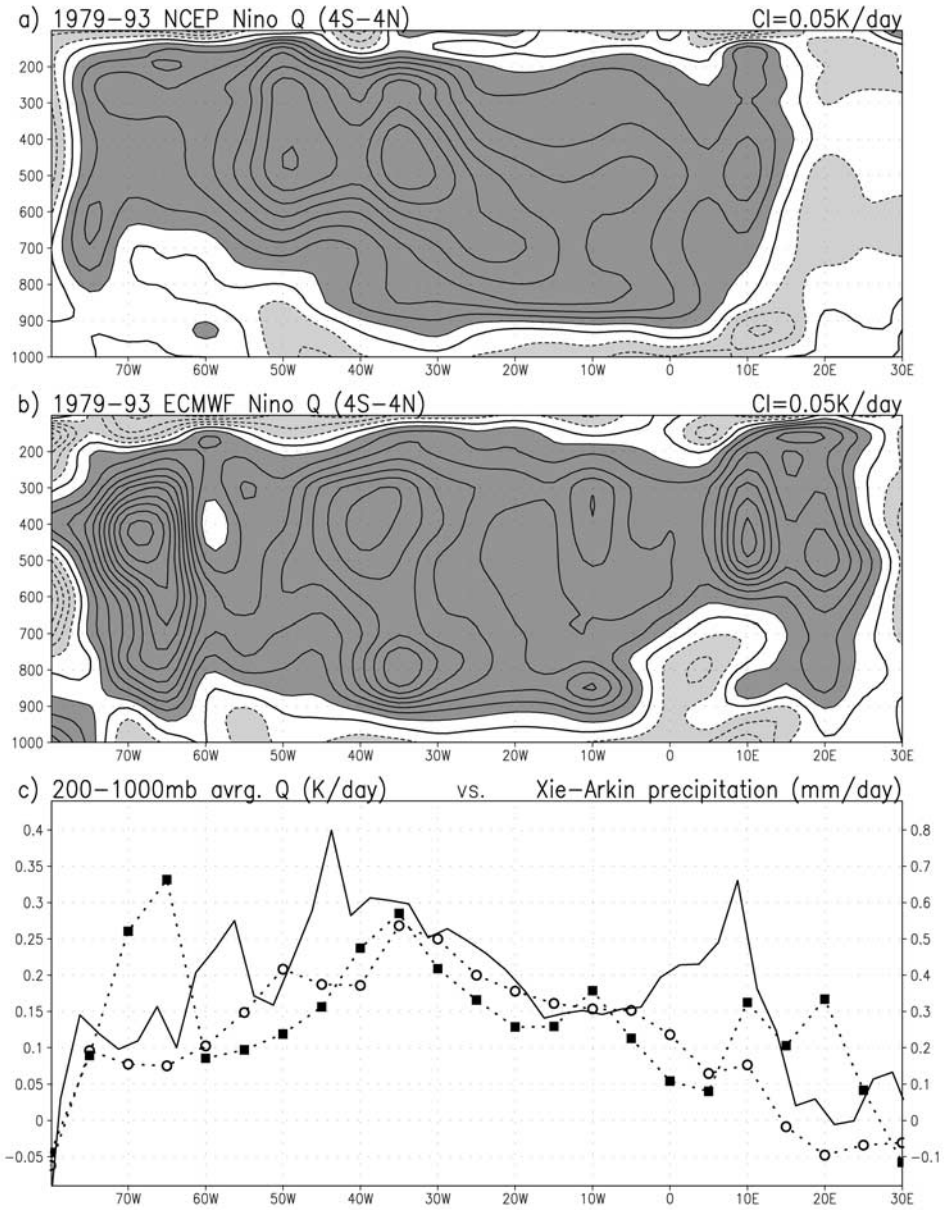

Figure 5. Equatorial (4°S–4°N) diabatic heating linked to Atlantic Niño variability; 3-D heating is residually diagnosed from the 1979–93 reanalysis data (a) from NCEP reanalyses and (b) from ECMWF reanalyses. The contour interval and shading threshold is 0.05 K/day in Figures 5a and 5b. Figure 5c shows the distribution of the mass-weighted vertically averaged (200–1000 mb) diabatic heating (left-scale in K/day) and Xie-Arkin precipitation (right-scale in mm/day), all in the 4°S–4°N equatorial band: NCEP heating (open circles), ECMWF heating (solid squares), Xie-Arkin precipitation (solid line). The CPC Merged Analysis of Precipitaton (CMAP) is referred to as Xie-Arkin precipitation in this study.

[35] An empirical model for the Atlantic surface-winds is also developed here. The distinguishing feature of the present analysis is the demonstration of potential superiority of this model over the simplified dynamical atmospheric models in the tropical Atlantic basin. The model is based on the rotated principal component analysis of internally driven wind variability. This variability component was defined in section 3, and extracted from the original (detrended) monthly SST and wind anomaly records by subtracting the variability associated with 15 modes that were identified as externally driven (because of large α values). The empirical model calculates the surface wind anomalies as follows: Monthly SST anomalies are first projected onto the SST components of the internally driven modes. Since these modes are obtained from rotated analysis, the loading vectors (SST + u + v) are no longer spatially orthogonal (even if they were orthogonal, their SST components need not be so), and the projections are thus calculated using the least squares method applied over the SST sub-space of the internally driven modes, as discussed more fully in *Chung and Nigam* [1999b, see section 4c]. The projection coeffi-

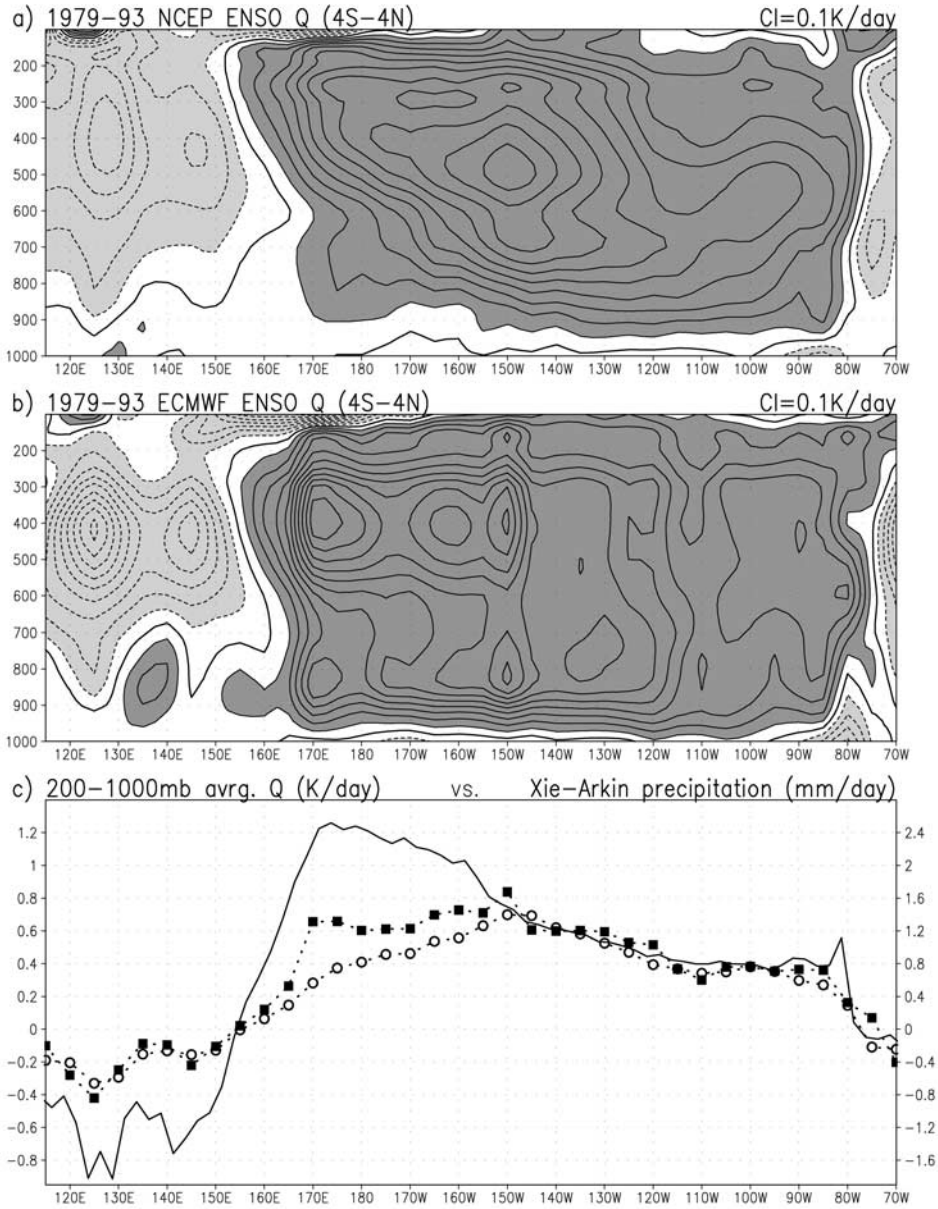

Figure 6. As in Figure 5, but for El Niño Southern Oscillation (ENSO) variability in the equatorial Pacific. Note that contour interval and shading threshold in Figure 6a and 6b (0.1 K/day) is twice as large as that in Figure 5.

cients are then used to construct the associated surface wind anomalies.

[36] The empirical modeling strategy is reasonably straightforward, but some issues need to be resolved before an optimum model can be realized. For example, should the principal component analysis of internally driven variability be performed for each calendar month, each season, or for all months together? How many leading modes should be rotated and retained for anomaly projection? These issues are investigated by constructing models based on (1) 20 modes extracted from rotated analysis of interannual variability of all calendar months together, (2) 20 modes from rotated analysis of monthly variability in each season (or, 80 modes annually), and (3) 10 modes from rotated analysis of variability in each calendar month (or, 120 modes annually). In case 3, 10 (and not 20) modes are rotated as the number of monthly anomalies analyzed is only 44, in contrast to 132 in the seasonal and 528 in the all-month cases.

[37] The empirical model's performance is evaluated from temporal correlation of the modeled and internally driven surface-wind anomalies in the 180-month period (1979–93). The period begins in 1979 so that performance of the empirical and Gill models can be compared; the Gill model is driven here by OLR anomalies, which are available continuously only since 1979. Correlation maps are generated for both the zonal and meridional wind components. Performance is assessed in each case (i.e., all-month, seasonal, and calendar month based models) for configurations based on 4-to-20 leading modes in cases 1–2, and

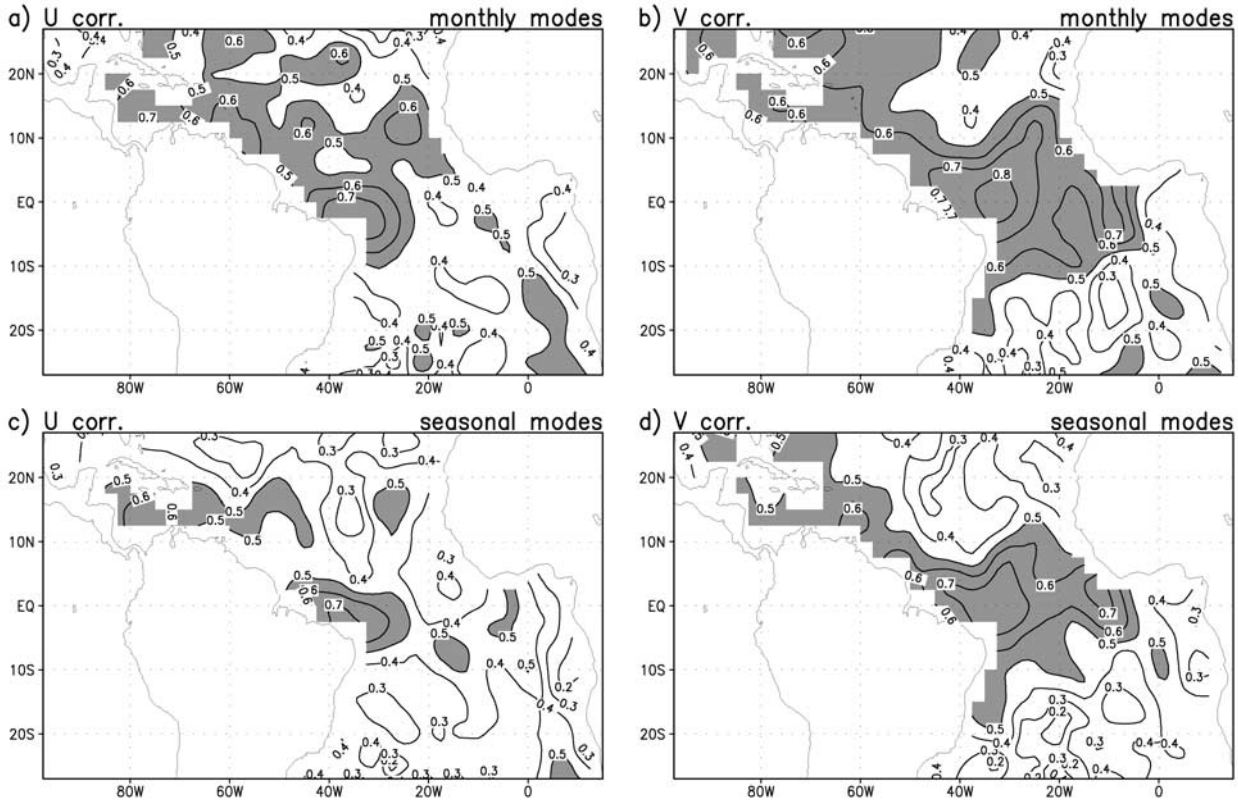

Figure 7. Empirical model's performance during January 1979–December 1993, from temporal correlation of the modeled and target wind anomalies. Performance of the model based on 10 internally driven modes of each calendar month (or 120 modes annually) is shown in Figures 7a and 7b, while that of the model based on 20 internally driven modes of each season is shown in Figures 7c and 7d. Contour interval is 0.1, and correlations greater than 0.5 are shaded in all panels. Compare this Figure 7 to Figure 9.

up to 10 modes in case 3. The model accuracy generally improves with the number of modes. The model based on modes of each calendar month was found to perform the best (and the one based on seasonal analysis, case 2, followed). The optimum model is thus based on 10 monthly modes (or, 120 modes annually). This model outperformed another based on the same number of degrees of freedom—a model based on 120 rotated modes extracted from an all-month analysis.

[38] The optimum model's performance is shown in the top two panels of Figure 7. The regions where wind correlations exceed 0.5 are shaded in each panel. The meridional wind simulation (Figure 7b) is quite good, particularly, in the equatorial (10°N–10°S) Atlantic where temporal correlation with the target anomalies generally exceeds 0.6. The zonal wind simulation (Figure 7a) is also satisfactory, although not quite as good as the meridional one. In both cases, the simulation is notably deficient in the equatorial southeastern Atlantic. The model's performance, when evaluated over the entire 44-year record (1950–93; 528 months; not shown) is somewhat better everywhere, and especially, in the southeastern sector.

[39] The bottom panels (Figures 7c–7d) display the performance of the empirical model based on modes from seasonal analysis. Comparison of the upper and lower panels indicates the marginally superiority of the model based on each calendar month modes.

[40] The optimum model was also used to compute the Atlantic surface wind anomalies in a specific month, August 1987. Both the detrended and the internally driven anomalies in this month were displayed earlier (Figures 2a–2b); the target for the optimum model is Figure 4b. The optimum model solution (Figure 8a) is spatially more coherent, and compares quite favorably with the target in much of the tropical Atlantic. The converging meridional winds, and zonal westerlies in the central/eastern equatorial Atlantic are well captured in the empirical solution, but the modeled winds in the Caribbean region are too strong and more easterly than in Figure 4b.

6. Performance of Simplified Dynamical Models

[41] The empirical model's performance is compared with that of simplified dynamical models assuming that the latter can be applied everywhere in the tropical Atlantic sector. Since such unrestricted application of the models is not permitted by the premises of the Gill and Lindzen-Nigam models (discussed briefly in the introduction)—the two simplified models considered in this study—comparisons with their performance across the tropical Atlantic are unfair,

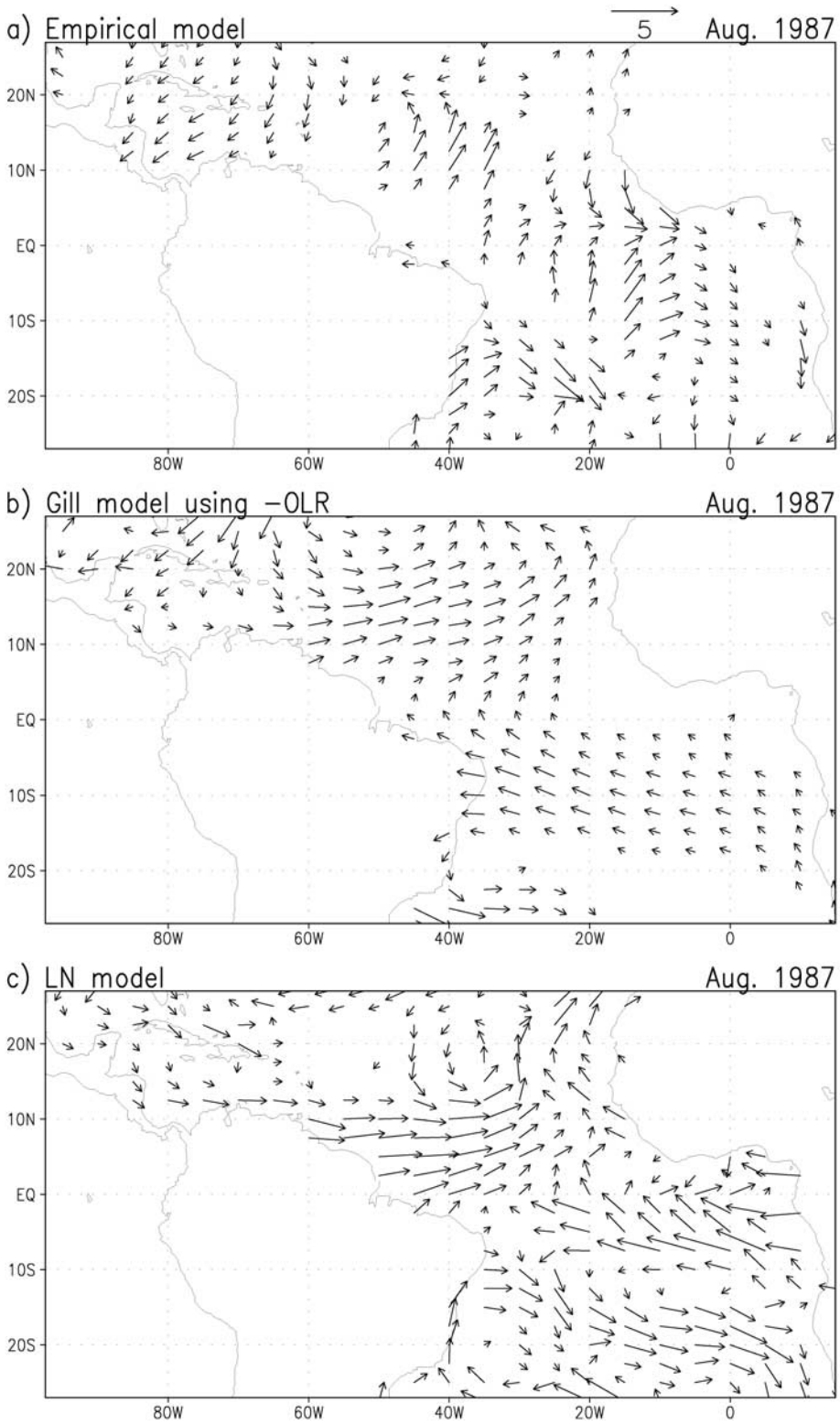

Figure 8. Modeling of August 1987 surface-wind anomalies using (a) the empirical model based on monthly modes (or 120 modes annually), (b) Gill model forced by this month's OLR anomalies, and (c) the Lindzen-Nigam model forced by this month's COADS SST. The modeling target is displayed in Figure 4b.

in principle. However, as a better comparison strategy proved difficult to devise, we apply the models across the tropical Atlantic, recognizing that the Lindzen-Nigam model's domain should be confined to the central/eastern sectors, and the Gill model's to the western/central sectors of the tropical Atlantic.

[42] The Gill model is forced by the monthly OLR anomalies during 1979–93; OLR has been used as proxy for the deep heating distribution in this model before [e.g., *Zhang and Krishnamurti*, 1996; *Nigam and Shen*, 1993]. The OLR anomalies over the oceanic sector were computed relative to the 1979–93 climatology, and the component linked to the internally driven surface wind variability was used as model-forcing in order to be consistent with the empirical model. This component was extracted by subtracting the OLR regressions of the 15 externally driven modes of Atlantic surface wind variability from the original OLR anomalies. Linear regressions against truncated principal components were computed, as in case of the diabatic heating anomalies.

[43] The Gill model solutions were obtained using Rayleigh dissipation and Newtonian cooling coefficients, both $(2\ \text{days})^{-1}$, and shallow-water gravity wave speed of 60 m/s—all as in *Zebiak and Cane* [1987]. The model was solved on a $2.5° \times 2.5°$ grid in the rectangular domain (97.5°W–15°E; 30°S–30°N), retaining full variation of the Coriolis force ($\sin\theta$). Field derivatives at the domain boundary were approximated using forward/backward differencing, and time integration was used to obtain the steady solution. Since the model is linear, and the model performance gauged by temporal correlation with the target fields during the 180-month period, little effort was expended in finding the optimum scaling factor. The model solution shown in Figure 8b was forced by the August 1987 OLR anomalies (in W/m^2), using a scaling factor of (1.08×10^{-3}).

[44] The Lindzen-Nigam model is forced by the SST-anomaly gradient. Again, the component linked to internally driven surface wind variability is used in order to be consistent with the empirical model. The model is solved in the same domain, and on the same grid as the Gill model. Model solution and subsequent inter-comparisons are facilitated by casting the Lindzen-Nigam model equations in the Gill format [*Neelin*, 1989]. The continuity equation in this version can be written as: $gH_o(u_x + v_y) + \varepsilon_c\varphi = -Sg\varepsilon_c(\text{SST})$. Note that in this version, a SST-proportional term forces the continuity equation, instead of SST-gradients forcing the horizontal momentum equations, as in the original Lindzen-Nigam model. The model was solved using the same Rayleigh momentum dissipation as in the Gill model $[(2\ \text{days})^{-1}]$, and $\varepsilon_c = (30\ \text{min})^{-1}$ and $H_o = 3$ Km. *Lindzen and Nigam* [1987] used these parameter values to simulate the climatological surface winds in the tropical Pacific. Again, little effort was spent in finding the optimum parameter values for the central/eastern portion of the tropical Atlantic basin. The August 1987 solution, shown in Figure 8c, was computed using $S = 12.0$.

[45] The dynamical model solutions in August 1987 (Figures 8b–8c) are spatially quite coherent, but differ in several respects, both among themselves and relative to the target (Figure 4b). The Gill model generates strong westerlies in the 10°–20°N belt, while the Lindzen-Nigam model produces such winds in the 0°–10°N sector, with the target feature being somewhere in between. The latter model produces notable winds in the eastern equatorial sector, particularly, meridional ones, but both dynamical models are unable to capture the prominent south-westerly anomalies in the central Atlantic (in Figure 4b). In the southern tropics, the dynamical responses are coherent but at odds with the target, which appears rather incoherent at the basin-scale.

[46] The performance of dynamical models was assessed more comprehensively, by computing model solutions in each of the 180 months (January 1979–December 1993), just as for the empirical model. Performance is evaluated again using temporal correlation of the modeled and target fields, which circumvents the need for extensive tuning of the response amplitude. Zonal and meridional wind correlations are plotted in Figure 9, with the Gill model ones in the top panels. A comparison of zonal-wind correlations shows that Gill model does better in the Caribbean region, and in the western equatorial sector, where diabatic heating is generally deeper and stronger. The Gill model is evidently not suitable over the tropical southeastern Atlantic, where zonal-wind correlations are negative. The Lindzen-Nigam model is comparatively better on account of positive correlations (> 0.3), but the empirical model is perhaps the best in this region (see Figure 7a). Comparison of the meridional-wind correlations confirms this assessment: The Lindzen-Nigam model outperforms the Gill model across the equatorial Atlantic sector, with correlations larger than 0.5 evident even in the eastern sector. But again, the empirical model is even better as the shaded area denoting correlations > 0.5 is much more expansive in Figure 7b, particularly in the latitudes. The large correlations in the Caribbean region are especially noteworthy.

[47] The simple dynamical models we tested performed poorly outside of the equatorial region, whereas the empirical model's performance was not found to degrade as strongly with latitude. One reason for such disparity in performance is the likely presence of the barotropic component in the atmospheric response to tropical Atlantic SST anomalies. In a GCM study, *Okumura et al.* [2001] found the SST anomalies to induce a large barotropic response in the subtropical Azores high region.

7. Summary and Concluding Remarks

[48] Modeling of the SST-forced surface winds—a critical coupling in ocean-atmosphere models—is quite challenging in the Atlantic basin. Simple dynamical models developed for the tropical Pacific surface winds are not directly applicable in the Atlantic in view of the basin's different geometry and size. The protruding South American and African landmasses in the Southern and Northern Tropics exert substantial influence on surface-wind variability in the tropical Atlantic, with potential feedback—warranting additional modeling consideration of the interaction of ocean and atmosphere with the adjoining continents. The tropospheric heating vertical structure also varies significantly across the basin, with the heating-maximum occurring in the lower troposphere in the eastern Atlantic. Not surprisingly, simple dynamical models have seen limited application in the tropical Atlantic [e.g., *Zebiak*, 1993; *Wagner and DaSilva*, 1994].

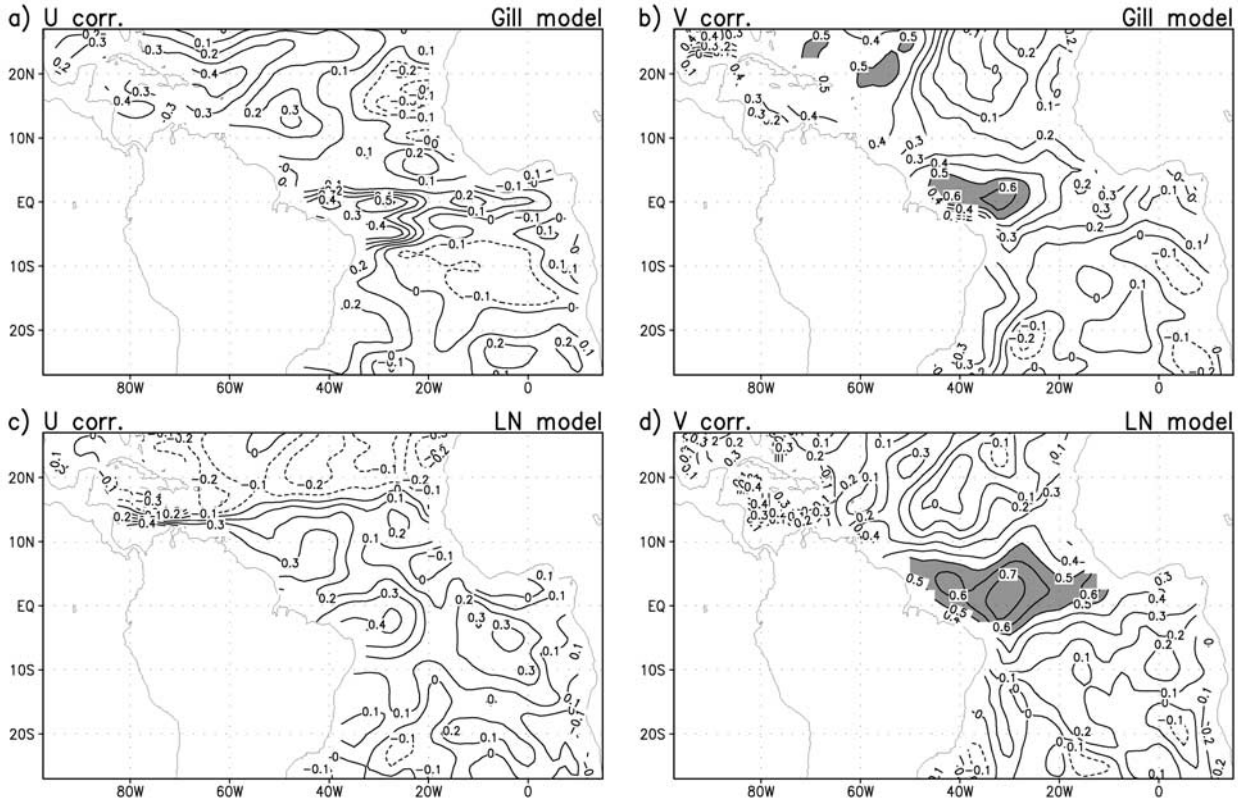

Figure 9. Performance of simplified dynamical models during January 1979–December 1993, from temporal correlation of the modeled and target wind anomalies: (a, b) Gill model forced by the internally driven OLR anomalies and (c, d) the Lindzen-Nigam model forced by COADS SST anomalies. Contour interval is 0.1, and correlations greater than 0.5 are shaded in all panels. Compare with Figures 7a–7b.

[49] Here, we seek to construct an empirical model for surface winds forced by the tropical Atlantic SSTs (i.e., for the internally driven component of tropical Atlantic wind variability), and investigate its performance vis-a-vis that of simple dynamical models, such as the Gill and Lindzen-Nigam models. Of necessity, a procedure is first developed to separate the internally driven component of surface winds from variability induced by changes external to the tropical Atlantic basin. This in itself was non-trivial as SST and surface wind observations were not available at sub-monthly resolution (e.g., weekly), in which case the lead/lag relationships could have been exploited. A separation strategy based on the very different ratios of the wind-to-SST amplitudes in modes obtained from the rotated principal component analysis of combined SST and wind variability was thus employed. Analysis of *DaSilva et al.*'s [1994] COADS data set showed that the internally driven component was dominant only within the equatorial sector (10°S–10°N) of the Atlantic, but across the tropics (30°S–30°N) in the Pacific.

[50] An empirical (statistical) model for the tropical Atlantic surface-winds was constructed from the extracted internally driven component of wind variability. The construction of an empirical model of surface wind/windstress is not novel in itself as such models have been developed for the tropical Pacific [*Syu et al.*, 1995], and even tropical Atlantic [*Chang et al.*, 1997]. The distinguishing feature of the present analysis is its focus on the *internally* driven wind component, and demonstration of this model's capacity vis-a-vis the simplified dynamical atmospheric models.

[51] The empirical model is based on the rotated principal component analysis of internally driven variability in the tropical Atlantic basin. Sensitivity to several analysis features was investigated in order to optimize the model's performance: For example, the combined variability analysis was conducted in each calendar month, each season, and all months together, and the number of modes rotated in each of these analyses was additionally varied. The optimum model was based on separate analysis of each calendar month's variability (10 rotated modes per calendar month). This model outperformed all other empirical model configurations, including the one based on 120 rotated modes from an all-month analysis.

[52] The empirical model's meridional wind simulation (Figure 7b) in the equatorial zone is striking. The Gill and Lindzen-Nigam models also do better in this field (Figures 9b and 9d), but they are evidently not quite competitive: Meridional wind correlations of the Lindzen-Nigam model (the better of the two dynamical models in the equatorial Atlantic) are in the 0.5–0.7 range while those of the empirical model (Figure 7b) are between 0.6–0.8. It is however in the modeling of zonal-winds that the empirical model does substantially better: Zonal wind correlations are

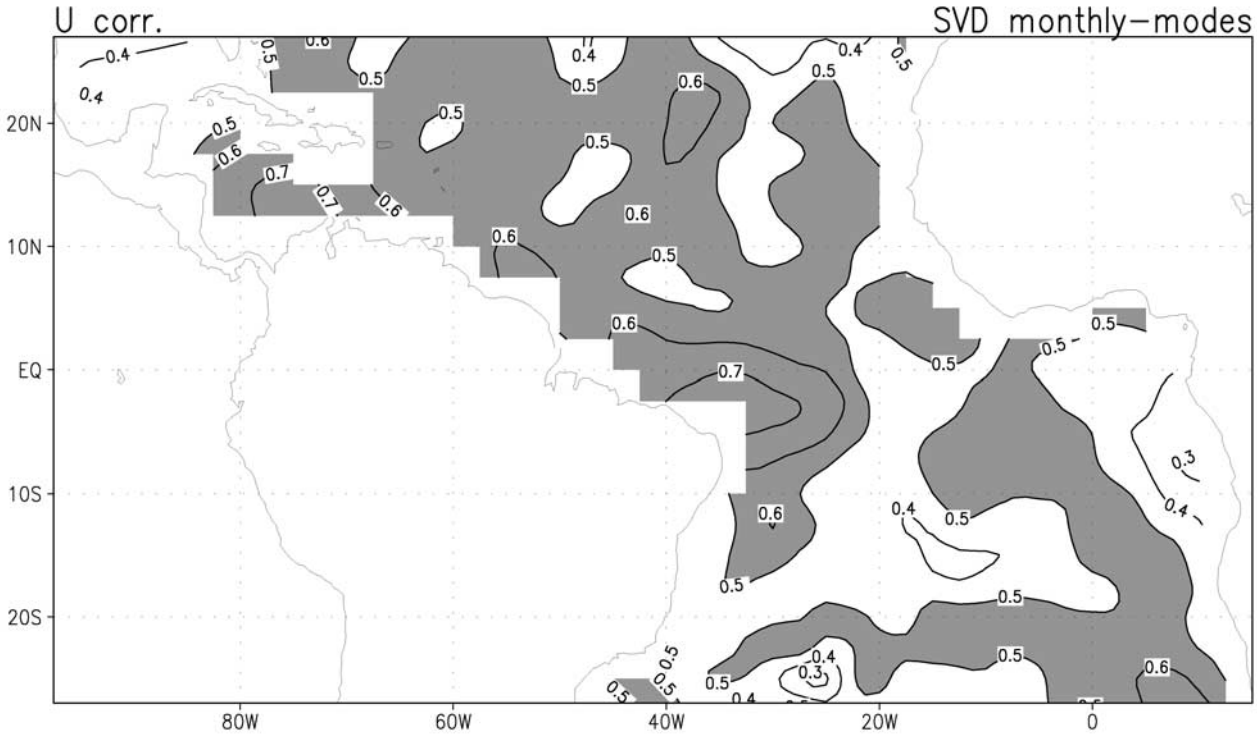

Figure 10. SVD-based empirical model's performance during January 1979–December 1993, from temporal correlation of the modeled and target zonal-wind anomalies. Performance of the model based on10 internally driven modes of each calendar month (or 120 modes annually).

in the 0.4–0.7 range, but only between −0.1 and 0.5 in case of the dynamical models.

[53] The dynamical models were solved across the tropical Atlantic basin, but such unrestricted application is not permitted by the models' premises. The Gill model is more valid in the western sector where the heating-maximum is higher (in the mid-troposphere), while the Lindzen-Nigam model is more valid in the central/eastern sectors under the subsiding branches of the divergent circulations. It is noteworthy that the empirical model outperforms the dynamical models even in these sectors.

[54] Finally, it would be interesting to compare the empirical model developed in this study with other such models. *Chang et al.* [1997] developed an empirical model for Atlantic surface winds based on the singular value decomposition analysis of SST and surface winds. Unfortunately, they did not document the model's performance, at least, using the measures used here. Moreover, these authors did not focus on the internally driven component of wind variability. This precluded a direct comparison of the two empirical models' performance. However, given our considerable interest in such comparison, we proceeded to construct a singular value decomposition based empirical model for zonal wind, keeping the latter as left variable and SST as the right variable in the analysis; only the internally driven component of COADS wind variability during 1950–93 was analyzed. The analysis was done for each calendar month, retaining 10 modes, all as before, so that model comparisons are as fair as possible. This model's performance was also evaluated during 1979–93, and the zonal wind correlations during this 180-month period are shown in Figure 10. Comparisons with Figure 7a, which displays performance of the RPCA based model, shows the empirical models to have rather similar potential, and in both cases more than those of dynamical models. That the differences in empirical models' performance are small relative to the performance enhancements over the dynamical models is noteworthy.

[55] The dynamical models could be further optimized by tuning model parameters, but their performance is unlikely to surpass those of empirical models. If anything, this points to the challenging nature of the problem (of modeling surface winds), due to the necessity of dealing with planetary boundary layers of various types, among others. The simplified dynamical models are useful pedagogical paradigms, but some shortcomings begin to surface as quantitatively accurate solutions are demanded.

[56] **Acknowledgments.** This effort was supported by NOAA Grant NA76GP0479 to Sumant Nigam, and NSF Grant OCE9812404 to James Carton. The research grew out of Chul Chung's Ph.D. dissertation which was submitted to the University of Maryland in January 1999. The authors thank Eric DeWeaver for local archiving of the NCEP reanalysis data set and for the diagnosis of 3D diabatic heating from it. They would also like to thank Alfredo Ruiz-Barradas for valuable discussions.

References

Barnett, T. P., M. Latif, N. E. Graham, M. Flügel, S. Pazan, and W. White, ENSO and ENSO-related predictability, Part I, Prediction of equatorial Pacific sea surface temperature with a hybrid coupled ocean-atmosphere model, *J. Clim.*, *6*, 1545–1566, 1993.

Battisti, D. S., E. S. Sarachik, and A. C. Hirst, A consistent model for the large-scale steady surface atmospheric circulation in the tropics, *J. Clim.*, *12*, 2956–2964, 1999.

Carton, J., and B. Huang, Warm events in the tropical Atlantic, *J. Phys. Oceanogr.*, *24*, 888–903, 1994.

Carton, J., X. Cao, B. S. Giese, and A. M. da Silva, Decadal and interannual SST variability in the tropical Atlantic ocean, *J. Phys. Oceanogr.*, *26*, 1165–1175, 1996.

Chang, P., L. Ji, and H. Li, A decadal climate variation in the tropical Atlantic ocean from thermodynamic air-sea interactions, *Nature*, *385*, 516–518, 1997.

Chang, P., L. Ji, and R. Saravanan, A hybrid coupled model study of tropical Atlantic variability, *J. Clim.*, *14*, 361–390, 2001.

Chiang, J. C. H., S. E. Zebiak, and M. A. Cane, Relative roles of elevated heating and surface temperature gradients in driving anomalous surface winds over tropical oceans, *J. Atmos. Sci.*, *58*, 1371–1394, 2001.

Chung, C., and S. Nigam, Weighting of geophysical data in principal component analysis, *J. Geophys. Res.*, *104*, 16,925–16,928, 1999a.

Chung, C., and S. Nigam, Asian summer monsoon—ENSO feedback on the Cane-Zebiak model ENSO, *J. Clim.*, *12*, 2787–2807, 1999b.

Clarke, A. J., and A. Lebedev, Long-term changes in the equatorial Pacific trade winds, *J. Clim.*, *9*, 1020–1029, 1996.

Da Silva, A. M., C. C. Young, and S. Levitus, *Atlas of Surface Marine Data 1994*, vol. 1, *Algorithms and Procedures, NOAA Atlas NESDIS 6*, 83 pp., Natl. Oceanic and Atmos. Admin., Washington, D.C., 1994.

Dommenget, D., and M. Latif, Interannual to decadal variability in the tropical Atlantic, *J. Clim.*, *13*, 777–792, 2000.

Enfield, D. B., and D. A. Mayer, Tropical Atlantic sea surface temperature variability and its relation to El Nino Southern Oscillation, *J. Geophys. Res.*, *102*, 929–945, 1997.

Gill, A. E., Some simple solutions for heat-induced tropical circulations, *Quart. J. Roy. Meteorol. Soc.*, *106*, 447–462, 1980.

Horel, J. D., A rotated principal component analysis of the interannual variability of the Northern Hemisphere 500 mb height field, *Mon. Weather Rev.*, *109*, 2080–2092, 1981.

Hoskins, B. J., On the existence and strength of the summer subtropical anticyclones, *Bull. Amer. Meteorol. Soc.*, *77*, 1287–1292, 1996.

Kalnay, E., et al., The NCEP/NCAR 40-year reanalysis project, *Bull. Amer. Meteorol. Soc.*, *77*, 437–471, 1996.

Klein, S. A., B. J. Soden, and N.-C. Lau, Remote sea surface temperature variations during ENSO: Evidence for a tropical atmospheric bridge, *J. Clim.*, *12*, 917–932, 1999.

Lanzante, J. R., Lag relationships involving tropical sea surface temperatures, *J. Clim.*, *9*, 2568–2578, 1996.

Lindzen, R. S., and S. Nigam, On the role of sea surface temperature gradients in forcing low-level winds and convergence in the tropics, *J. Atmos. Sci.*, *44*, 2440–2458, 1987.

Mehta, V. M., Variability of the tropical ocean surface temperatures at decadal-multidecadal timescales, Part I, The Atlantic Ocean, *J. Clim.*, *11*, 2351–2375, 1998.

Merle, J., Annual and interannual variability of temperature in the eastern equatorial Atlantic ocean –Hypothesis of an Atlantic El Nino, *Oceanol. Acta*, *3*, 209–220, 1980.

Moura, A. D., and J. Shukla, On the dynamics of droughts in northeast Brazil — Observations, theory, and numerical experiments with a general circulation model, *J. Atmos. Sci.*, *38*, 2653–2675, 1981.

Neelin, D. J., On the interpretation of the Gill model, *J. Atmos. Sci.*, *46*, 2466–2468, 1989.

Nigam, S., and Y. Chao, Evolution-dynamics of tropical ocean-atmosphere annual-cycle variability, *J. Clim.*, *9*, 3187–3205, 1996.

Nigam, S., and C. Chung, ENSO surface winds in CCM3 simulation: Diagnosis of errors, *J. Climate*, *13*, 3172–3186, 2000.

Nigam, S., and H.-S. Shen, Structure of oceanic and atmospheric low-frequency variability over the tropical Pacific and Indian ceans, Part I, COADS observations, *J. Clim.*, *6*, 657–676, 1993.

Nigam, S., C. Chung, and E. DeWeaver, ENSO diabatic heating in ECMWF and NCEP reanalyses, and NCAR CCM3 simulation, *J. Clim.*, *13*, 3152–3171, 2000.

Okumura, Y., S.-P. Xie, A. Namaguti, and Y. Tanimoto, Tropical Atlantic air-sea interaction and its influence on the NAO, *Geophys. Res. Lett.*, *28*, 1507–1510, 2001.

Philander, S. G. H., Unusual conditions in the tropical Atlantic Ocean in 1984, *Nature*, *322*, 236–238, 1986.

Philander, S. G. H., *El Niño, La Niña and the Southern Oscillation, Int. Geophys. Ser.*, vol. 46, 293 pp., Academic, San Diego, Calif., 1990.

Ruiz-Barradas, A., J. Carton, and S. Nigam, Coupled climate modes in the tropical Atlantic sector, *J. Clim.*, *13*, 3285–3297, 2000.

Syu, H.-H., J. D. Neelin, and D. Gutzler, Seasonal and interannual variability in a Hybrid Coupled GCM, *J. Clim.*, *8*, 2121–2143, 1995.

Tanimoto, Y., and S.-P. Xie, Ocean-atmosphere variability over the Pan-Atlantic basin, *J. Meteorol. Soc. Jpn.*, *77*, 31–46, 1999.

Wagner, R. G., and A. M. DaSilva, Surface conditions associated with anomalous rainfall in the Guinea coastal region, *Intl. J. Climatol.*, *14*, 179–199, 1994.

Xie, P., and P. A. Arkin, Global Precipitation: A 17-year monthly analysis based on gauge observations, satellite estimates, and numerical model outputs, *Bull. Amer. Meteorol. Soc.*, *78*, 2539–2558, 1997.

Xie, S.-P., and K. Saito, Formation and variability of a northerly ITCZ in a hybrid coupled AGCM: Continental forcing and oceanic-atmosphere feedback, *J. Clim.*, *14*, 1262–1276, 2001.

Xie, S.-P., and Y. Tanimoto, A pan-Atlantic decadal climate oscillation, *Geophys. Res. Lett.*, *25*, 2185–2188, 1998.

Zebiak, S. E., Air-sea interaction in the equatorial Atlantic region, *J. Clim.*, *6*, 1567–1586, 1993.

Zebiak, S. E., and M. A. Cane, A model El Niño Southern Oscillation, *Mon. Wea. Rev.*, *115*, 2262–2278, 1987.

Zhang, Z., and T. N. Krishnamurti, A generalization of Gill's heat-induced tropical circulation, *J. Atmos. Sci.*, *53*, 1045–1052, 1996.

J. Carton and S. Nigam, Department of Meteorology, Room 3403, Computer and Space Sciences Building, University of Maryland, College Park, MD 20742-2425, USA. (nigam@atmos.umd.edu)

C. Chung, Center for Clouds, Chemistry, and Climate, Scripps Institution of Oceanography, La Jolla, CA 92037-0239, USA.